

# Using Recurrent Neural Networks to Optimize Dynamical Decoupling for Quantum Memory

Moritz August<sup>\*1</sup> and Xiaotong Ni<sup>\*2</sup>

<sup>1</sup>Department of Informatics, Technical University of Munich, 85748 Garching, Germany (august@in.tum.de)

<sup>2</sup>Max-Planck Institute for Quantum Optics, 85748 Garching, Germany (xiaotong.ni@mpq.mpg.de)

May 28, 2022

## Abstract

We utilize machine learning models which are based on recurrent neural networks to optimize dynamical decoupling (DD) sequences. DD is a relatively simple technique for suppressing the errors in quantum memory for certain noise models. In numerical simulations, we show that with minimum use of prior knowledge and starting from random sequences, the models are able to improve over time and eventually output DD-sequences with performance better than that of the well known DD-families. Furthermore, our algorithm is easy to implement in experiments to find solutions tailored to the specific hardware, as it treats the figure of merit as a black box.

## 1 Introduction

A major challenge of quantum information processing (e.g. quantum computation and communication) is to preserve the coherence of quantum states. While in principle we can build a fault-tolerant quantum memory or universal quantum computer once the error rate of the device is below a certain threshold, it is still beyond nowadays experimental capacity. One less explored area is the optimization of implementing the fault-tolerant protocol on a concrete experimental setting. This is often a tedious problem, due to the amount of details in the real devices, and the fact that the architectures of both experimental devices and theoretical protocols are still rapidly changing. Thus, an attractive approach is to

---

\*These two authors contributed equally.

automatize this optimization task. Apart from convenience, it is conceivable that with less human intuition imposed, the upper bound of the performance will be higher. This has previously been proven to be true in fields such as computer vision where artificial neural network (ANN) models that try to solve tasks without using hand-crafted representations of data have overtaken approaches based on human insight in tasks like image classification and object recognition [24]. Another interesting recent example is the ability of ANNs to learn how to play games on a human or even super-human level without any or just little prior knowledge about the respective games [27, 41].

Automatically optimizing parameters in real (or numerical simulations of) experiments is not a new idea. For example, it has been applied to optimizing the pulse shape of a laser, the parameters of Hamiltonians to achieve certain unitary operations or parameters of dynamical decoupling and cold atom experiments. Most works that attempt to obtain optimal parameters use genetic algorithms [19, 14, 10, 30] (and to some degree [23]) or local searches such as gradient descent [5, 8, 30, 2, 26] and the Nelder-Mead simplex method [4, 9, 21]. It is argued that by using these optimization methods directly on the experiments, we can avoid the hardness of modelling the imperfect control and the system-environment interaction. However, one possible weakness of these optimization methods is that they generate new trials only by looking at a fixed number of previous ones, and often they need to restart once they reach a local minimum. Thus, in the long run, they do not fully utilize all the data generated by the experiments.

In this work, we propose an orthogonal approach, where we build a model that approximates the generating distribution of good parameters. After an initial optimization, this model can then be used to efficiently generate new possible trials and can be continuously updated based on new data. In particular, we choose this model to be a variant of the recurrent neural network (RNN), which makes our approach very similar to the way in which natural languages or handwriting are currently modelled. This ansatz enables us to exploit the models and insights developed by the machine learning community and possibly translate further progress there into the field of quantum control. It is worth pointing out that the machine learning part of this work is purely classical; only the (classical) data are related to quantum time evolution (see Figure 1 for a possible workflow). Among the previous work, the approach in [52] is the most similar to ours, as they attempt to build a model from the data and utilize the model to perform optimization. (Classical) machine learning is also used in [6, 29, 47] to characterize the error models in quantum error correction and to react accordingly.

To demonstrate the feasibility of using our method to help optimizing quantum memory, we consider the problem of automatically learning and optimizing dynamical decoupling sequences (almost) without using any prior knowledge. Dynamical decoupling (DD) [49] is a technique which combats certain noise by applying a sequence of unitary operations on the system (see [44, 35] for a review). It has a less stringent requirement compared to general error correction protocols, which allows it to be demonstrated in experiments [4, 25, 44] in contrast to other methods. Moreover, DD-sequences have a relatively simple structure, and therefore it is conceivable that a learning algorithm could eventually sample them without the need of using heavy mathematics.

## 2 Background

### 2.1 Dynamical decoupling

The majority of dynamical decoupling schemes are designed for error models where the system-environment interaction can be described by a Hamiltonian. We will use  $\mathcal{H}_S$  and  $\mathcal{H}_B$  to denote the Hilbert space of the system and environment (often called bath), respectively. The difference between system and environment is that the former represents the part of the Hilbert space we can apply the Hamiltonian on and in which we store quantum information. The total noise Hamiltonian is

$$H_0 = H_S \otimes I_B + I_S \otimes H_B + H_{SB}.$$

Without intervention, in general  $H_0$  would eventually destroy the quantum states we store on  $\mathcal{H}_S$ . To suppress this noise, we could apply a time dependent Hamiltonian  $H_C(t)$  to the system, which makes the total Hamiltonian  $H(t) = H_0 + H_C(t)$ . In the ideal case, we can control the  $H_C(t)$  perfectly and reach very high strength (i.e. norm of the Hamiltonian), which allows the ideal pulse

$$V(t) = O\delta(t - t_0).$$

It applies a unitary operator  $e^{-iO}$  to the system for an infinitely small duration (we set  $\hbar = 1$  in this work). A very simple DD-scheme for a qubit (a two level system  $S$ ) is the  $XY_4$  sequence: it applies pulses of the Pauli-matrices  $X$  and  $Y$  alternately with equal time interval  $\tau_d$  in between. A complete cycle consists of four pulses  $XYXY$ , thus the total time period of a cycle is  $T_c = 4\tau_d$ . In the limit of  $\tau_d \rightarrow 0$ , the qubit can be stored for an arbitrarily long time. The intuition behind DD-sequences is the average Hamiltonian theory. Let  $U_C(t) = \mathcal{T} \exp\{-i \int_0^t dt' H_C(t')\}$  be the total unitary applied by  $H_C(t')$  up to time  $t$ . In the interaction picture defined by  $U_C(t)$ , the dynamics is governed by the Hamiltonian  $\tilde{H}(t) = U_C^\dagger(t) H_0 U_C(t)$ . If the time interval  $\tau_d$  between pulses is much smaller than the time scale defined by the norm of  $\|H_0\|$ , it is reasonable to consider the average of  $\tilde{H}(t)$  within a cycle. The zeroth-order average Hamiltonian in  $T_c$  (with respect to  $\tau_d$ ) is

$$\bar{H}^{(0)} = \frac{1}{T_c} \int_0^{T_c} dt' U_C^\dagger(t') H_0 U_C(t').$$

For the  $XY_4$  sequences introduced above, it is easy to compute  $\bar{H}^{(0)} = \frac{1}{4} \sum_{\sigma \in \{I, X, Y, Z\}} \sigma H_0 \sigma$ . Since the mapping  $O \rightarrow \sum_{\sigma \in \{I, X, Y, Z\}} \sigma O \sigma$  maps any  $2 \times 2$  matrix to 0, by linearity we know  $\bar{H}^{(0)} = 0$ . More DD sequences are introduced in Appendix A.

However, we cannot expect these requirements to be met in all real world experiments. The two major imperfections that are often studied are the flip-angle errors and the finite duration of the pulses. Flip-angle errors arise from not being able to control the strength and time duration of  $H_C(t)$  perfectly, thus the intended pulse  $V(t) = O\delta(t)$  becomes  $V(t) = (1 \pm \epsilon)O\delta(t)$ . And since zero-width pulses  $O\delta(t)$  are experimentally impossible, we must consider finite-width pulses which approximate the ideal ones. In this paper, we will only consider the imperfection of finite-width pulses. However, it is straightforward to apply our algorithm to pulses with flip-angle errors.

## 2.2 Measure of performance

There are multiple ways to quantify the performance of DD-sequences. In practice, we choose different measures to suit the intended applications. Here we use the same measure as in [35], which has the advantage of being (initial) state-independent and having a closed formula for numerical simulation:

$$D(U, I) = \sqrt{1 - \frac{1}{d_S d_B} \|\text{Tr}_S(U)\|_{\text{Tr}}}$$

where  $U$  represents the full evolution operator generated by  $H(t)$ ,  $d_S$  and  $d_B$  are the dimensions of the system and environment Hilbert space  $\mathcal{H}_S$  and  $\mathcal{H}_B$ , respectively.  $\|X\|_{\text{Tr}} = \text{Tr}(\sqrt{X^\dagger X})$  is the trace-norm, and  $\text{Tr}_S(\cdot)$  is the partial trace over  $\mathcal{H}_S$ . The smaller  $D(U, I)$  is, the better the system preserved its quantum state after the time evolution. For example, the ideal evolution  $U = I_S \otimes U_B$  has the corresponding  $D(U, I) = 0$ .

In experiments, it is very hard to evaluate  $D(U, I)$ , as we often do not have access to the bath's degree of freedom. Instead, the performance of DD-sequences is often gauged by doing process tomography for the whole time duration where DD is applied [25, 43]. Although it is a different measure compared to our choice above, the optimization procedure can still be applied as it does not rely on the concrete form of the measure. Moreover, for solid state implementations such as superconducting qubits or quantum dots, a typical run of initialization, applying DD-sequences and measurements can be done on the time scale of 1 ms or much faster. Thus, it is realistic that on the time scale of days we can gather a large dataset of DD-sequences and their performance, which is needed for our algorithm.

## 2.3 Recurrent Neural Networks

Sequential models are widely used in machine learning for problems with a natural sequential structure, e.g. speech and handwriting recognition, protein secondary structure prediction, etc. For dynamical decoupling, not only do we apply the gates sequentially in the time domain, but also the longer DD sequences are often formed by repetition or concatenation of the short ones. Moreover, once the quantum information of the system is completely mixed into the environment, it is hard to retrieve it again by DD. Thus, an educated guess is that the performance of a DD-sequence largely depends on the short subsequences of it, which can be modelled well by the sequential models.

Since our goal is not simply to approximate the distribution of good dynamical decoupling sequences by learning their structure but to sample from the learned distribution to efficiently generate new good sequences, we will further restrict ourselves to the class of generative sequential models. Overall, these models try to solve the following problem: given  $\{x_i\}_{i < t}$ , approximate the conditional probability  $p(x_t | x_{t-1}, \dots, x_1)$ . As a simple example, we can estimate the conditional probability  $p(x_t | x_{t-1})$  from a certain data set, and

Model	Starting from Section 3, a model is a particular instance of a long short-term memory network, which is explained in detail in Appendix F.2.
Topology	The topology of a neural network specifies how the network is connected, including the dimension of each node. For example, see Figure 8.
Optimization parameters	The parameters which decide how the stochastic gradient descent algorithm <i>Adam</i> runs (e.g. learning rates).

Table 1: Terminology for Section 3 and 4

use it to generate new sequences<sup>1</sup>. For more sophisticated problems (e.g. natural language or handwriting), it is not enough to only consider the nearest neighbour correlations as simple models like Markov-chains of order one do.

The long short-term memory (LSTM) network, a variation of the recurrent neural network (RNN), is a state-of-the-art technique for modelling longer correlations [12] and is comparably easy to train. The core idea of RNNs is that the network maintains an internal state in which it encodes information from previous time steps. This allows the model to, at least theoretically, incorporate all previous time steps into the output for a given time. Some RNNs have even been shown to be Turing-complete [34]. In practice, however, RNNs often can only model relatively short sequences correctly due to an inherently unstable optimization process. This is where LSTMs improve over normal RNNs, as they allow for training of much longer sequences in a stable manner. Furthermore, LSTMs, like all ANNs, are based on matrix multiplication and the element-wise application of simple non-linear functions. This makes them especially efficient to evaluate.

From the machine learning perspective, we treat the problem at hand as a supervised learning problem where we provide the model with examples that it is to reproduce according to some error measure. We do not use the framework of reinforcement learning since the performance of a DD-sequence could only be measured after the whole sequence is applied. A short introduction to machine learning, LSTMs and their terminology can be found in the appendix and in [28] while a more exhaustive discussion can be found in [13, 11].

### 3 Algorithm

The algorithm presented in this section is designed with the goal in mind to encode as little prior knowledge about the problem into it as possible, in order to make it generally

<sup>1</sup>This idea can be at least dated back to Shannon [40], where this model generated “English sentences” like “ON IE ANTSOUTINYS ARE T INCTORE ST BE S DEAMY ACHIN D ILONASIVE TUCCOOWE AT....”

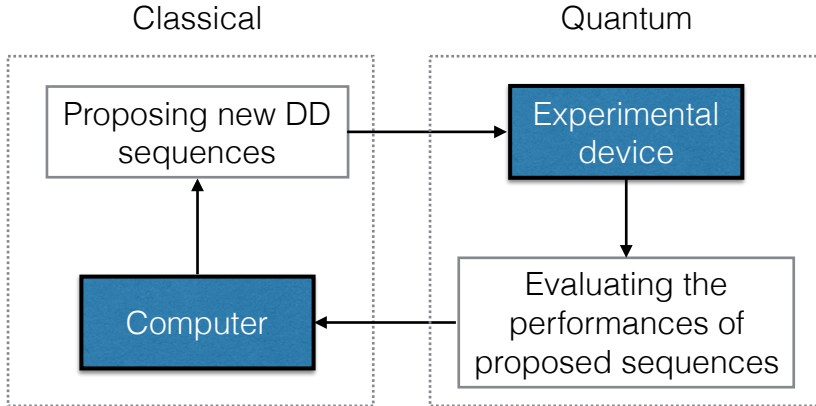


Figure 1: A flowchart of how our algorithm can be used to optimize DD-sequences for real experimental devices. However, for this paper, we have replaced the experimental part with numerical simulation.

applicable. Following this idea, the method is agnostic towards the nature of the considered gates, the noise model and the measure of performance. To implement this, the algorithm assumes that

- the individual gates are represented by a unique integer number such that every sequence  $s \in \mathcal{G}^{\otimes L_s}$  with  $\mathcal{G}$  denoting the set of the unique identifiers and  $L_s$  being the length of  $s$ .
- it is provided with a function to compute the score  $\zeta_s$  of a given sequence  $s$  taking into account the noise model.

We will now first present the outline of the basic algorithm before explaining each step in more detail. Some useful terminology can be found in Table 1.

The algorithm consists of two nested optimization-loops, where the inner loop fits a number of recurrent neural networks to the current data while the outer loop uses the output of the inner loop to optimize the average score of the training data. This works as follows:

1. An initial database of  $d$  random sequences together with their scores is created. The best  $p$  percent of the sequences are taken as the initial training data.
2. In the inner loop, multiple recurrent neural network models with varying topologies and optimization parameters (see Appendix F) are fitted to the training data.
3. The trained models are ranked according to the average score  $\langle \zeta \rangle$  of the sequences they generate and the top  $k$  models are selected.
4. The selected models are used to generate a new database of  $d$  sequences and scores. The best  $p$  percent of the data are used to define a new training set. The outer loop jumps to step 2.

---

**Algorithm 1:** General Optimization Algorithm

---

**Input** : Number of models to train:  $n$ , Number of models to keep:  $k$ , Percentage of data to keep:  $p$ , Set of possible topologies:  $\mathcal{M}$ , Size of data:  $d$

- 1  $D \leftarrow \text{generateRandomData}(d)$  ;
- 2  $D, \langle \varsigma \rangle \leftarrow \text{keepBestData}(D, p)$  ;
- 3 **while**  $\langle \varsigma \rangle$  *not converged* **do**
- 4      $M \leftarrow \text{trainRandomModels}(n, D, \mathcal{M})$  ;
- 5      $M \leftarrow \text{keepBestKModels}(M, k)$  ;
- 6      $D \leftarrow \text{generateDataFromModels}(M, d)$  ;
- 7      $D, \langle \varsigma \rangle \leftarrow \text{keepBestData}(D, p)$  ;
- 8 **end**

**Output:**  $\langle \varsigma \rangle, D, M$

---

The basic method is shown in Algorithm 1. The individual steps will now be elaborated on in greater depth.

**Generation of the initial training data** The size  $d$  and the quality, i.e. the percentage  $p$  of the initial data to be kept, are the parameters which we can specify. The data are then generated by sampling a gate from the uniform distribution over all gates for each time-step. The average score  $\langle \varsigma \rangle$  of the initial data can then be used as a baseline to compare against in case no other reference value is available.

**Training of the RNNs** To reduce the chance of ending up in a bad local optimum, for each training set several different topologies of LSTMs are trained. These topologies are randomly sampled from the set of possible topologies  $\mathcal{M}$ . The training problem is defined by assuming a multinoulli distribution over the gates of each time step and minimizing the corresponding negative log-likelihood  $-\sum_t \delta_{s_t, i} \log p_i(s_{t-1}, \dots, s_1)$ , where  $i$  is the index of the correct next gate,  $p_i$  is its predicted probability computed by the LSTM and  $\delta_{s_t, i} = 1$  iff  $s_t = i$ . This means that the LSTM is asked to predict  $s_t$  from  $s_{t-1}, \dots, s_1$  with high probability. The optimization is done by stochastic gradient descent (see appendix F.3 for further details and terminology), or more exactly the approximate second-order method *Adam* [22], which has proven to be quite robust in stochastic optimization of neural networks.

**Selecting the best models** While we train the models to reproduce the distribution of the training data, this is not what we actually want to achieve. Instead, we want to find the distribution that produces the sequences with the best scores. So, we rank the trained models according to the average score of a fixed number of generated sequences and choose the best  $k$  of them. We do not directly optimize the LSTM to produce sequences with good scores since it is not clear whether this can be done efficiently, especially in the case where the scores are provided by experimental devices. Furthermore, a direct optimization of the score would possibly yield LSTMs which generate homogeneous DD sequences. It should be kept in mind that a desired feature of the models is the ability to generate sequences with large variety. For example, a model which remembers the best sequence of a dataset

---

**Algorithm 2:** Optimization Algorithm with reused Models

---

**Input** : Number of initial models to train:  $n$ , Number of models to keep:  $k$ ,  
Percentage of data to keep:  $p$ , Set of possible topologies:  $\mathcal{M}$ , Size of data:  $d$

- 1  $D \leftarrow \text{generateRandomData}(d)$  ;
- 2  $D, \langle \varsigma \rangle \leftarrow \text{keepBestData}(D, p)$  ;
- 3  $M \leftarrow \text{trainRandomModels}(n, D, \mathcal{M})$  ;
- 4  $M \leftarrow \text{keepBestKModels}(M, k)$  ;
- 5 **while**  $\langle \varsigma \rangle$  *not converged* **do**
- 6      $M \leftarrow \text{trainBestModels}(D)$  ;
- 7      $D \leftarrow \text{generateDataFromModels}(M, d)$  ;
- 8      $D, \langle \varsigma \rangle \leftarrow \text{keepBestData}(D, p)$  ;
- 9 **end**

**Output:**  $\langle \varsigma \rangle, D, M$

---

and uses it as the sole output will have a very good average score, but is useless for our purpose. This relation between the average score and variety of solution can be viewed as the “exploitation vs. exploration trade-off” (see [36]). However, we find that the LSTMs in our experiments are able to generate new and diverse sequences, thus we only use the average score over the generated sequences as benchmark for selecting models.

**Generation of the new training data** The selected models are used to generate  $d$  new training data by sampling from their distributions. This is done by randomly choosing a gate for the first time step and feeding it into the model. From the output-distribution  $p(x_2|x_1)$ , a gate for the next time step is sampled which is in turn used as input for the next step. This is iterated until a sequence of the desired length is obtained. The generated sequences are again ordered by their scores and the best  $p$  percent are chosen for the next iteration of the optimization.

The algorithm described above imposes as little prior knowledge as possible and tries to minimize the bias in the optimization. Among other things, this comes at the cost of having to train a larger number of models from scratch for each new data set. If one is however willing to accept a more biased optimization for the sake of a significant speed-up, a way to achieve this is to reuse the best models in each iteration:

In the first step, a larger number of  $n$  models is trained on the initial data and the best  $k$  topologies are selected. In the remaining generations, instead of randomly sampling new topologies of models, the already selected ones are trained on the better data and then used again to generate new training data. It is obvious that this variant is much more prone to ending up in a bad local optimum. On the other hand side, it drastically reduces the number of models to be trained. This scheme of alternatingly fixing the data to optimize the models and consecutively fixing the models to optimize the data resembles the probabilistic model building genetic algorithm [32] and to some extent the expectation-maximization algorithm [7]. This variant is shown in Algorithm 2. Another way of speeding up the algorithm is to combine the data of previous iterations with the newly generated data to



possibly achieve a better average score of the best  $p$  percent. As the data generated by the models should become better in each iteration, the effect of also considering old data might however be very small.

As a last remark we would like to point out that, especially when one wants to optimize longer sequences, an alternative way to generate the initial data is by using the models trained on shorter sequences. This approach could lead to an initial data set with much higher average score, but at the price of introducing the bias from the previously trained RNNs.

## 4 Numerical Results

### 4.1 Noise model and the control Hamiltonian

Throughout the paper, we will use the same noise model as in [35]. We consider a 1-qubit system and a 4-qubit bath, namely  $\dim(\mathcal{H}_S) = 2$  and  $\dim(\mathcal{H}_B) = 16$ . The small dimension of the bath is for faster numerical simulation, and there is no reason for us to think that our algorithm would only work for a small bath as the size of the bath enters the algorithm only via the score-computation function (see Appendix C.2 for more discussion). The total noise Hamiltonian consists of (at most) 3-body interactions between the system and bath-qubits with random strength:

$$H_0 = \sum_{\mu \in \{I, X, Y, Z\}} \sigma^\mu \otimes B_\mu, \quad (1)$$

where  $\sigma^\mu$  is summed over Pauli-matrices on the system-qubit. And  $B_\mu$  is given by

$$B_\mu = \sum_{i \neq j} \sum_{\alpha, \beta} c_{\alpha\beta}^\mu \left( \sigma_i^\alpha \otimes \sigma_j^\beta \right),$$

where  $i, j$  is summed over indices of the bath qubits, and  $\sigma_i^{\alpha(\beta)}$  is the Pauli-matrix on qubit  $i$  of the bath. We consider the scenario where the system-bath interaction is much stronger than the pure bath terms. More precisely, we set  $c_{\alpha\beta}^\mu \approx 1000c_{\alpha\beta}^I$  for  $\mu \in \{X, Y, Z\}$ . Apart from this constraint, the absolute values  $|c_{\alpha\beta}^\mu|$  are chosen randomly from a range  $[a, b]$ , where we set  $b \approx 3a$  to avoid too many terms vanishing in (1). The result Hamiltonian has a 2-norm  $\|H_0\| = 20.4$ .

For the control Hamiltonian, we consider the less explored scenario where the pulse shape have finite width but no cool down time between them (100% duty cycle). In other words, the control Hamiltonian is piecewise constant

$$H_C(t) = H_k, \quad \text{for } k\tau_d \leq t < (k+1)\tau_d,$$

where  $\tau_d$  is a small time period with respect to the norm of  $H_0$ , and  $e^{-iH_k\tau_d} \in \{I, X, Y, Z\}$ . This is a good toy model for experimental settings whose DD-performance is mainly limited by the strength of the control Hamiltonian, but not the speed of shifting between

Hamiltonians. Since this regime is less explored in theoretical studies, it is an interesting scenario to explore via machine learning. Another restriction we put on  $H_C(t)$  is

$$H_C(t) = -H_C(T - t) ,$$

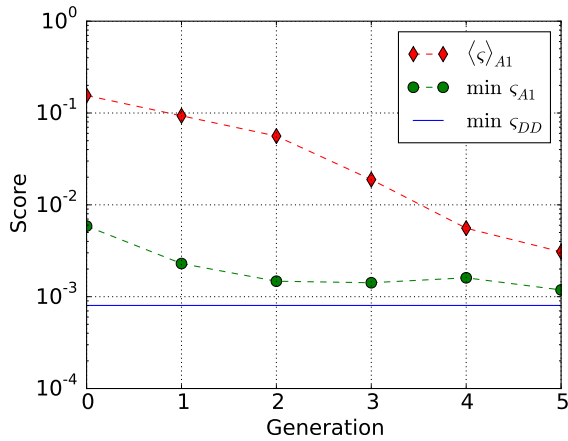
where  $T$  is the total evolution time. This condition ensures  $U_C(T) = \mathcal{T} \exp\{-i \int_0^T dt H_C(t)\} = I$ , and it allows us to apply the same code on the setting where the system has more than one qubit. It is known that this family of symmetric Hamiltonians can remove the first order terms of  $\tau_d$  in the average Hamiltonian[49, 42]. So strictly speaking, this should be counted as prior knowledge. However, when we compare the known DD-sequences with the numerically found ones, we also use the symmetric version of the known DD-sequences. Thus, we perform the comparison on equal terms.

## 4.2 Experiments

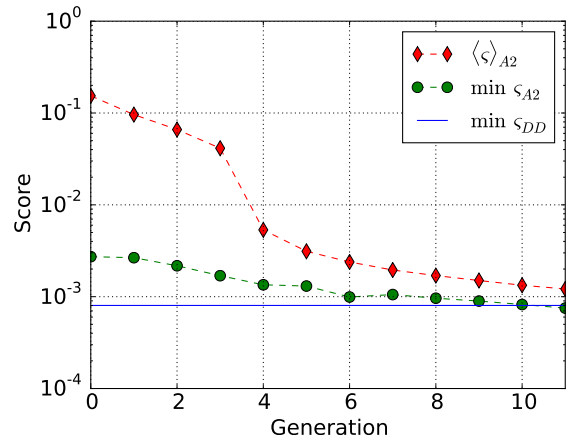
In the following, we present results of three experiments that we have conducted to evaluate the performance of our method. In the first experiment, we have used Algorithm 1 to establish a baseline. In a second experiment, we compared the results of Algorithm 1 and 2 for the same problem parameters. In a third experiment, we evaluated Algorithm 2 for a more difficult scenario. Additional experiments were done to test the applicability of our method to further problem settings, see Appendix B.

**Experiment 1** To generally verify that Algorithm 1 works as intended, we considered sequences of 32 gates with  $\tau_d = 0.004$ . We let the algorithm train  $n = 100$  models for each generation. All models are trained for 100 epochs, i.e. complete iterations over the data set, which means every sequence in the dataset is used 100 times during the stochastic optimization. We set the number of generations  $k = 5$  and always chose the best 10% of the data generated by each model, such that we obtained a training set of  $d = 10,000$  sequences for each generation. The topologies of the RNNs were composed of at most three LSTM-layers with optionally allowed peepholes (see appendix for further details on the topologies). Between each pair, a linear down-projection was placed. These layers were finally followed by a softmax-layer to generate the required probability-distribution. The first LSTM-layer was defined to have the largest number of dimensions that then successively decreased in the following layers and projections down to the number of gates in the final layer. The maximal number of dimensions was set to 500. In addition to the architectures of the models, the optimization parameters such as batch-size, initial learning rate and the parameters specific to *Adam* were randomly chosen from a set of reasonable values. The DD32-scheme was found to yield the best sequence as was chosen as reference. The results are shown in Table 2 and the convergence illustrated in Figure 2a.

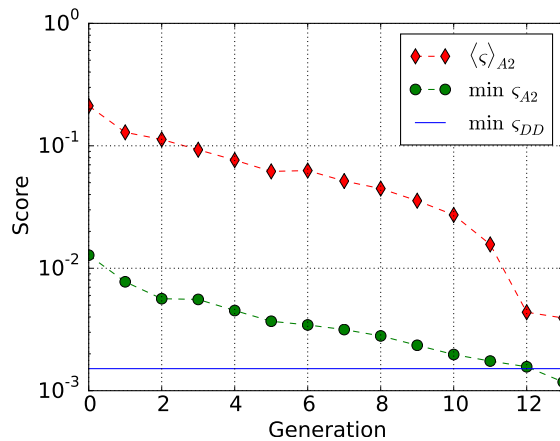
The results show that the last training set consists of sequences with better average scores compared to known DD-families. The best score of DD is however better than the one found by our algorithm, mainly due to the fact that the algorithm is only run for 5 generations (see the next experiment for a comparison). From the 10,000 sequences of the last generated data, every sequence was found to be unique. This indicates that our models



(a) Experiment 1



(b) Experiment 2



(c) Experiment 3

Figure 2: The three plots showing the convergence of the average and best scores of the data generated in Experiment 1-3. The average score is computed on the training data set of each generation, which is the top 10% sequences generated by the selected models. (For generation 0, instead the training data is the top 10% of randomly generated sequences). As a reference, also the best score obtained from DD is shown. The experiment 2 and 3 are stopped at the generations where the best scores surpass the known ones.

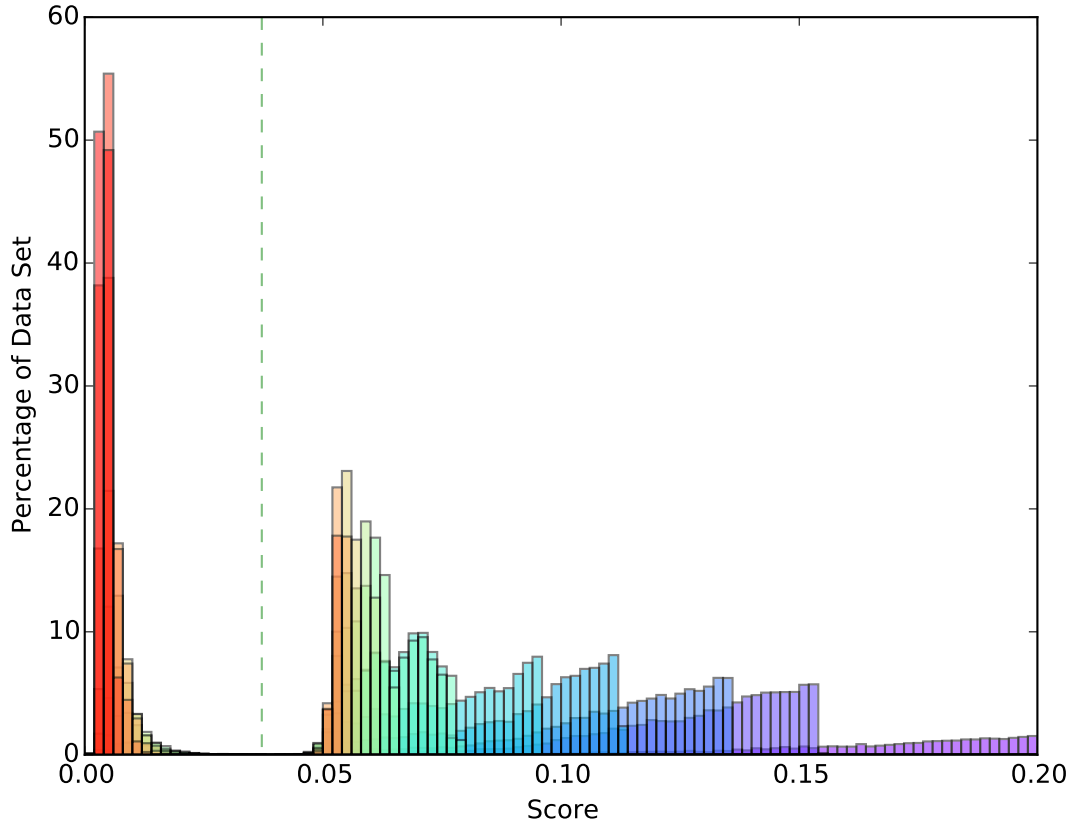


Figure 3: An illustration of the score distributions over the training sets of all generations of Experiment 3. The color indicates the generation of the data, from purple for the initial data to bright red for the last generation. Each generation contains 20,000 sequences. The clear gap between scores is likely due to the fact that DD sequences can be classified according to the order of noise they can suppress (see [35]). The green dashed line shows the average of top 10% scores which were generated from a trained model in the last generation of Experiment 2. Thus, in order to reduce the time needed for optimization, we have the option to use models trained for short sequences to generate the initial dataset of longer ones.

Sequences	$\langle \varsigma \rangle$	min $\varsigma$
CDD32	0.053250	<b>0.000803</b>
CDD4	0.482037	0.456539
CDD8	0.002934	0.002586
EDD8	<b>0.002398</b>	0.002112
CDD16	0.043202	0.001170
CDD64 (no reverse)	0.016005	0.001078
Last training set	0.0030802	0.001185
Best model	0.028331	-
Random	0.341667	-

Table 2: A comparison of sequences generated in Experiment 1 and known DD-families (see Appendix A). We use the distance  $D$  defined in Section 2.2 to compute the scores of sequences (thus the smaller the better). The last training set consists of the top 10% sequences generated by the best five models in the last generation. Apart from CDD64, the sequences consist of 32 gates. (Thus, in total all sequences have 64 gates as length-32 sequences are then reversed, see section 4.1).  $\tau_d$  was set to 0.004. For the DD-families and the training data, also the best score is reported. The best results are printed bold.

do indeed learn a meaningful internal representation of good sequences and do not only try to reproduce a few good ones. The high diversity of the sequences might for instance allow for further statistical analysis to infer characteristics of the good sequences (see [20] for examples of analyzing RNNs’ inner mechanisms). The plots also show that our strategy of choosing the best  $p\%$  of the generated data leads to a relatively nice convergence-behaviour. Note that the difference between average and minimal score decreases over the generations.

**Experiment 2** In our next experiment, we wanted to compare the Algorithms 1 and 2. So, we chose to consider the same scenario as for the last experiment, but this time employing Algorithm 2. We let it train an initial set of 50 models and chose the five best topologies to be reused for all following generations. All other parameters were kept identical and we stopped the run after eleven generations. Figure 2b and Table 3 show the results.

It is clearly visible in the results that Algorithm 2 outperforms DD, achieving both a significantly better average and a slightly better minimal score. Again, all sequences of the final data were unique. In comparison to the basic version, it was able to improve upon its results due to the higher number of generations. Figure 2b illustrates that the convergence is similar compared to that of the basic version of the algorithm. It is however worth noting that this variant of the method obtained these better results by training only 100 models in total as compared to 500 and by that generating more than twice as many generations in about 20% of the runtime. These results show that already a small set of

Sequences	$\langle \varsigma \rangle$	min $\varsigma$
CDD32	0.053250	0.000803
Last training set	<b>0.001214</b>	<b>0.000751</b>
Best model	0.008227	-
Random	0.341667	-

Table 3: A comparison of sequences generated in Experiment 2 and known DD-families (see Appendix A). We use the distance  $D$  defined in Section 2.2 to compute the scores of sequences (thus the smaller the better). The sequences considered here consisted of 32 gates and  $\tau_d$  was set to 0.004. For the DD-family and the training data, also the best scores are reported. The best results are printed bold.

well-chosen topologies of models suffices for our method to generate state-of-the-art scores. Due to this significant advantage in efficiency, we consider Algorithm 2 to be superior and have used it for the following experiment.

**Experiment 3** In a third experiment we wanted to evaluate how Algorithm 2 performs on the more difficult problem of optimizing sequences with length 64 (hence a total length of 128 with the reversed half), gates with a time step of again  $\tau_d = 0.004$ . We kept most of the parameters for optimization and topology of the models as before, this time however generating 20,000 sequences for each training set and having the stochastic gradient descent method loop over the data set 200 times to account for the increased amount of possible sequences. The initial number of models to be trained was set to 30 and the best 5 topologies were then reused for all following 12 generations. We performed a truncation of the gradients to 32 time steps to avoid instabilities in the optimization (see Appendix F.3 of this paper or Section 3.2 of [12] for the details). Figure 2c and Table 4 show the results.

The results show that our method is capable of optimizing the best and average scores to a level that exceeds known DD-classes also for this scenario. As for the previous experiments, we find that all obtained sequences are unique. The convergence appears to be relatively stable albeit not very fast. This is however not surprising as we start the optimization from random sequences in a space of  $4^{64}$  possibilities.

One interesting aspect to note is an apparent jump of the average score between generation 11 and 12. That this jump is not a mere coincidence can be understood by examining Figure 3. It shows that there seems to be a sharp separation between the class of mediocre and the class of good sequences. Bridging this gap translates to accumulating enough sequences from the better regime in order to allow the models to learn their structure. It is a nice demonstration of the robustness of our method that it was apparently able to do this, explaining the sudden jump of the average score. However, as can be seen from the convergence-plot it took several generations to obtain enough sequences from the good regime.

It is likely that this phenomenon is not an artifact of our particular choice of parameters

Sequences	$\langle \varsigma \rangle$	min $\varsigma$
CDD32	0.106227	0.001607
CDD4	0.612311	0.591753
CDD8	0.005865	0.005172
EDD8	0.004793	0.004222
CDD16	0.085563	0.002339
CDD64	0.031547	0.001514
Last training set	<b>0.003925</b>	<b>0.001178</b>
Best model	0.057010	-
Random	0.44918	-

Table 4: A comparison of sequences generated in Experiment 3 and known DD-families (see Appendix A). We use the distance  $D$  defined in Section 2.2 to compute the scores of sequences (thus the smaller the better). The last training set consists of the top 10% sequences generated by the best five models in the last generation. The sequences consist of 64 gates. (Thus, in total all sequences have 128 gates as length-64 sequences are then reversed, see Section 4.1).  $\tau_d$  was set to 0.004. For the DD-families and the training data, also the best score is reported. The best results are printed bold.

in this experiment. Hence, choosing a better starting point for the optimization by using models trained on shorter sequences or randomly perturbed DD-sequences might be a good way of speeding up the convergence drastically. To test this idea, we chose the best model obtained in Experiment 2 and let it generate 2000 sequences of 64 gates. Of these sequences, we took the best 10% as we would have done if the data had been used for training. The obtained data was found to have an average score of 0.037175, which is about one order of magnitude better than the average of the initial training data generated from random sequences. Thus, we conclude that this approach is a viable option for speeding up the optimization process, however at the cost of possibly introduced bias.

We list the best sequences we obtained for the three above experiments in the appendix.

## 5 Conclusion

We have introduced a novel method for optimizing dynamical decoupling sequences, which differs from previous work by the ability to utilize much larger datasets generated during the optimization. Its ability to efficiently generate large sets of good sequences could be used along with other optimization methods to cover their weaknesses or to perform statistical analysis of these sequences. We show that for certain imperfect control Hamiltonians, our method is able to outperform (almost all) known DD-sequences. The little prior knowledge

about DD we use is (1) choosing Pauli operators as pulses in the sequences, see Experiment B2 in section B for more discussion, (2) choosing specific lengths for the DD-sequences and (3) enforcing the reversal symmetry, as discussed in section 4.1. However, we do not need to initialize the dataset in a specific way as in the Appendix C.5.a of [35], which actually contains a certain amount of prior knowledge of DD. Also, our method does not fundamentally rely on the prior knowledge stated above. It is conceivable that the use of this prior knowledge can be lifted, at the price of a possibly much slower optimization procedure. Thus, a possible direction of future research is to see how we can minimize the slow-down when not incorporating any prior knowledge and whether we can obtain good DD-sequences with non-Pauli pulses.

While we have applied the algorithm to the case of quantum memory and compared it to dynamical decoupling, it is of general nature. It can in principle be applied to every problem where the optimization of a sequence of gates with respect to some well-defined figure of merit is desired and where it is feasible to evaluate this performance measure for larger numbers of sequences. However, due to the nature of the underlying machine learning model, good results will likely only be obtained for problems whose solution depends strongly on local correlations in the sequences.

## Acknowledgements

We want to thank Geza Giedke for helpful discussions and comments on the draft. The idea of this paper partially stems from a discussion between Courtney Brell and Xiaotong Ni about using genetic algorithms to optimize quantum memory. This work was partly supported by the Elite Network of Bavaria through the doctoral programme 'Exploring Quantum Matter'.



## References

- [1] M. Abadi et al. “TensorFlow: Large-scale machine learning on heterogeneous systems, 2015”. In: *Software available from tensorflow.org* ().
- [2] L. Banchi, N. Pancotti, and S. Bose. “Quantum gate learning in engineered qubit networks: Toffoli gate with always-on interactions”. In: (2015), p. 5. arXiv:1509.04298. URL: <http://arxiv.org/abs/1509.04298>.
- [3] Y. Bengio and Y. LeCun. “Scaling learning algorithms towards AI”. In: *Large-scale kernel machines* 34.5 (2007).
- [4] M. J. Biercuk et al. “Optimized dynamical decoupling in a model quantum memory.” In: *Nature* 458.7241 (2009), pp. 996–1000. ISSN: 1476-4687. DOI: 10.1038/nature07951. URL: <http://dx.doi.org/10.1038/nature07951>.
- [5] C. Chen, L.-C. Wang, and Y. Wang. “Closed-loop and robust control of quantum systems.” In: *The Scientific World Journal* 2013 (2013), p. 869285. ISSN: 1537-744X. DOI: 10.1155/2013/869285. URL: <http://www.pubmedcentral.nih.gov/articlerender.fcgi?artid=3749599{\&}tool=pmcentrez{\&}rendertype=abstract>.
- [6] J. Combes et al. “In-situ characterization of quantum devices with error correction”. In: (2014). arXiv:1405.5656. URL: <http://arxiv.org/abs/1405.5656>.
- [7] A. P. Dempster, N. M. Laird, and D. B. Rubin. “Maximum likelihood from incomplete data via the EM algorithm”. In: *Journal of the royal statistical society. Series B (methodological)* (1977), pp. 1–38.
- [8] D. Dong et al. “Robust manipulation of superconducting qubits in the presence of fluctuations”. en. In: *Scientific Reports* 5 (2014), p. 7873. ISSN: 2045-2322. DOI: 10.1038/srep07873. arXiv:1408.1556. URL: <http://www.nature.com/srep/2015/150119/srep07873/full/srep07873.html><http://www.nature.com/articles/srep07873><http://arxiv.org/abs/1408.1556>.
- [9] P. Doria, T. Calarco, and S. Montangero. “Optimal control technique for many-body quantum dynamics.” In: *Physical review letters* 106.19 (2011), p. 190501. ISSN: 1079-7114. DOI: 10.1103/PhysRevLett.106.190501. URL: <http://journals.aps.org/prl/abstract/10.1103/PhysRevLett.106.190501>.
- [10] I. Geisel et al. “Evolutionary optimization of an experimental apparatus”. In: *Applied Physics Letters* 102.21 (2013), p. 214105. ISSN: 00036951. DOI: 10.1063/1.4808213. arXiv:1305.4094. URL: <http://arxiv.org/abs/1305.4094>.
- [11] I. Goodfellow, Y. Bengio, and A. Courville. “Deep Learning”. Book in preparation for MIT Press. 2016. URL: <http://goodfeli.github.io/dlbook/>.
- [12] A. Graves. “Generating Sequences With Recurrent Neural Networks”. In: *arXiv preprint arXiv:1308.0850* (2013). arXiv:1308.0850. URL: <http://arxiv.org/abs/1308.0850>.

- [13] K. Greff et al. “LSTM: A search space odyssey”. In: *arXiv preprint arXiv:1503.04069* (2015).
- [14] U. L. Heras et al. “Genetic Algorithms for Digital Quantum Simulations”. In: (2015). arXiv:1512.00674. URL: <http://arxiv.org/abs/1512.00674>.
- [15] S. Hochreiter and J. Schmidhuber. “Long short-term memory”. In: *Neural computation* 9.8 (1997), pp. 1735–1780.
- [16] K. Hornik. “Approximation capabilities of multilayer feedforward networks”. In: *Neural networks* 4.2 (1991), pp. 251–257.
- [17] K. Hornik, M. Stinchcombe, and H. White. “Multilayer feedforward networks are universal approximators”. In: *Neural networks* 2.5 (1989), pp. 359–366.
- [18] E. Jones, T. Oliphant, and P. Peterson. “{SciPy}: open source scientific tools for {Python}”. In: (2014).
- [19] R. Judson and H Rabitz. “Teaching lasers to control molecules.” In: *Physical review letters* 68.10 (1992), pp. 1500–1503. ISSN: 1079-7114. DOI: 10.1103/PhysRevLett.68.1500. URL: <http://journals.aps.org/prl/abstract/10.1103/PhysRevLett.68.1500>.
- [20] A. Karpathy. “The Unreasonable Effectiveness of Recurrent Neural Networks”. In: <http://karpathy.github.io/2015/05/21/rnn-effectiveness/> (2015).
- [21] J. Kelly et al. “Optimal quantum control using randomized benchmarking”. In: *Physical Review Letters* 112.24 (2014), pp. 1–5. ISSN: 10797114. DOI: 10.1103/PhysRevLett.112.240504. arXiv:1403.0035.
- [22] D. P. Kingma and J. Ba. “Adam: A method for stochastic optimization”. In: *International Conference on Learning Representation*. 2015.
- [23] M. Krenn et al. “Automated Search for new Quantum Experiments”. In: *Physical Review Letters* 116.9 (2016), p. 090405. ISSN: 0031-9007. DOI: 10.1103/PhysRevLett.116.090405. URL: <http://journals.aps.org/prl/abstract/10.1103/PhysRevLett.116.090405>.
- [24] A. Krizhevsky, I. Sutskever, and G. E. Hinton. “Imagenet classification with deep convolutional neural networks”. In: *Advances in neural information processing systems*. 2012, pp. 1097–1105.
- [25] G. de Lange et al. “Universal dynamical decoupling of a single solid-state spin from a spin bath.” In: *Science (New York, N.Y.)* 330.6000 (2010), pp. 60–63. ISSN: 0036-8075. DOI: 10.1126/science.1192739. arXiv:1008.2119.
- [26] S. Machnes et al. “Comparing, optimizing, and benchmarking quantum-control algorithms in a unifying programming framework”. In: *Physical Review A* 84.2 (2011), p. 022305.
- [27] V. Mnih et al. “Playing atari with deep reinforcement learning”. In: *arXiv preprint arXiv:1312.5602* (2013).

- [28] M. Nielsen. *Neural network and deep learning*. Determination Press, 2015.
- [29] D. Orsucci, M. Tiersch, and H. J. Briegel. “Estimation of coherent error sources from stabilizer measurements”. In: (2015). arXiv:1512.07083. URL: <http://arxiv.org/abs/1512.07083>.
- [30] L. Pawela and P. Sadowski. “Various methods of optimizing control pulses for quantum systems with decoherence”. In: *Quantum Information Processing* (2016). ISSN: 1570-0755. DOI: 10.1007/s11128-016-1242-y. URL: <http://link.springer.com/10.1007/s11128-016-1242-y>.
- [31] M. Pelikan. “Bayesian optimization algorithm”. In: *Hierarchical Bayesian optimization algorithm*. Springer, 2005, pp. 31–48.
- [32] M. Pelikan, D. E. Goldberg, and F. G. Lobo. “A survey of optimization by building and using probabilistic models”. In: *Computational optimization and applications* 21.1 (2002), pp. 5–20.
- [33] M. Pelikan and A. K. Hartmann. “Searching for ground states of Ising spin glasses with hierarchical BOA and cluster exact approximation”. In: *Scalable Optimization via Probabilistic Modeling*. Springer, 2006, pp. 333–349.
- [34] J. B. Pollack. *On connectionist models of natural language processing*. Computing Research Laboratory, New Mexico State University, 1987.
- [35] G. Quiroz and D. Lidar. “Optimized dynamical decoupling via genetic algorithms”. In: *Physical Review A - Atomic, Molecular, and Optical Physics* 88.5 (2013). ISSN: 10502947. DOI: 10.1103/PhysRevA.88.052306. arXiv:1210.5538.
- [36] H. Robbins. “Some aspects of the sequential design of experiments”. In: *Bulletin of the American Mathematical Society* 58.5 (1952), pp. 527–536. ISSN: 0002-9904. DOI: 10.1090/S0002-9904-1952-09620-8. URL: <http://www.ams.org/bull/1952-58-05/S0002-9904-1952-09620-8/>.
- [37] C. A. Ryan, J. S. Hodges, and D. G. Cory. “Robust decoupling techniques to extend quantum coherence in diamond”. In: *Physical Review Letters* 105.20 (2010), pp. 1–4. ISSN: 00319007. DOI: 10.1103/PhysRevLett.105.200402. arXiv:1008.2197.
- [38] D. Saad. *On-line learning in neural networks*. Vol. 17. Cambridge University Press, 2009.
- [39] H. Sak, A. Senior, and F. Beaufays. “Long short-term memory based recurrent neural network architectures for large vocabulary speech recognition”. In: *arXiv preprint arXiv:1402.1128* (2014).
- [40] C. Shannon. “A Mathematical Theory of Communication”. In: *Bell System Technical Journal* 27 (1948), 379–423, 623–656.
- [41] D. Silver et al. “Mastering the game of Go with deep neural networks and tree search”. In: *Nature* 529 (2016), pp. 484–503. URL: <http://www.nature.com/nature/journal/v529/n7587/full/nature16961.html>.

- [42] A. M. Souza, G. A. Álvarez, and D. Suter. “Effects of time-reversal symmetry in dynamical decoupling”. In: *Physical Review A* 85.3 (2012), p. 032306. ISSN: 1050-2947. DOI: 10.1103/PhysRevA.85.032306. arXiv:1110.1011. URL: <http://arxiv.org/abs/1110.1011>.
- [43] A. M. Souza, G. A. Álvarez, and D. Suter. “Robust dynamical decoupling.” In: *Philosophical transactions. Series A, Mathematical, physical, and engineering sciences* 370.1976 (2012), pp. 4748–69. ISSN: 1364-503X. DOI: 10.1098/rsta.2011.0355. arXiv:1110.6334. URL: <http://arxiv.org/abs/1110.6334>.
- [44] A. M. Souza, G. A. Alvarez, and D. Suter. “Robust dynamical decoupling for quantum computing and quantum memory.” In: *Physical review letters* 106.24 (2011), p. 240501. ISSN: 1079-7114. DOI: 10.1103/PhysRevLett.106.240501. URL: <http://journals.aps.org/prl/abstract/10.1103/PhysRevLett.106.240501>.
- [45] I. Sutskever et al. “On the importance of initialization and momentum in deep learning”. In: *Proceedings of the 30th international conference on machine learning (ICML-13)*. 2013, pp. 1139–1147.
- [46] T. Tieleman and G. Hinton. “Lecture 6.5-rmsprop: Divide the gradient by a running average of its recent magnitude”. In: *COURSERA: Neural Networks for Machine Learning* 4 (2012), p. 2.
- [47] M. Tiersch, E. J. Ganahl, and H. J. Briegel. “Adaptive quantum computation in changing environments using projective simulation.” In: *Scientific reports* 5 (2015), p. 12874. ISSN: 2045-2322. DOI: 10.1038/srep12874. arXiv:arXiv:1407.1535v1. URL: <http://www.nature.com/srep/2015/150811/srep12874/full/srep12874.html>.
- [48] S. Van Der Walt, S. C. Colbert, and G. Varoquaux. “The NumPy array: a structure for efficient numerical computation”. In: *Computing in Science & Engineering* 13.2 (2011), pp. 22–30.
- [49] L. Viola, E. Knill, and S. Lloyd. “Dynamical Decoupling of Open Quantum Systems”. In: *Physical Review Letters* 82.12 (1999), pp. 2417–2421. ISSN: 0031-9007. DOI: 10.1103/PhysRevLett.82.2417. URL: <http://journals.aps.org/prl/abstract/10.1103/PhysRevLett.82.2417>.
- [50] M. Welling and Y. W. Teh. “Bayesian learning via stochastic gradient Langevin dynamics”. In: *Proceedings of the 28th International Conference on Machine Learning (ICML-11)*. 2011, pp. 681–688.
- [51] P. J. Werbos. “Backpropagation through time: what it does and how to do it”. In: *Proceedings of the IEEE* 78.10 (1990), pp. 1550–1560.
- [52] P. B. Wigley et al. “Fast machine-learning online optimization of ultra-cold-atom experiments”. In: (2015), p. 6. arXiv:1507.04964. URL: <http://arxiv.org/abs/1507.04964>.

- [53] R. J. Williams and D. Zipser. “A learning algorithm for continually running fully recurrent neural networks”. In: *Neural computation* 1.2 (1989), pp. 270–280.

## A Dynamical decoupling sequences

In this section, we are going to list several classes of DD-sequences. We will first explain how to concatenate two sequences, as most long DD-sequences are constructed in this manner. Given two DD-sequences  $A = P_1 \cdots P_m$  and  $B = Q_1 \cdots Q_n$ , the concatenated sequence  $A[B]$  is

$$A[B] = (P_1 Q_1) Q_2 \cdots Q_n (P_2 Q_1) Q_2 \cdots Q_n \cdots (P_m Q_1) Q_2 \cdots Q_n$$

As an example, when we concatenate the length-2 and length-4 sequences  $XX$  and  $XYXY$ , we obtain  $IYXYIYXY$ .

We will use  $P_i$  to represent any Pauli matrix  $X$ ,  $Y$  or  $Z$ , and for  $i \neq j$ ,  $P_i \neq P_j$ . The families of DD-sequences can then be listed as the following:

**DD4** are length-4 sequences  $P_1 P_2 P_1 P_2$ .

**DD8** are length-8 sequences  $IP_2 P_1 P_2 IP_2 P_1 P_2$ .

**EDD8** are length-8 sequences  $P_1 P_2 P_1 P_2 P_2 P_1 P_2 P_1$

**CDD16** are length-16 concatenated sequences  $DD4[DD4]$

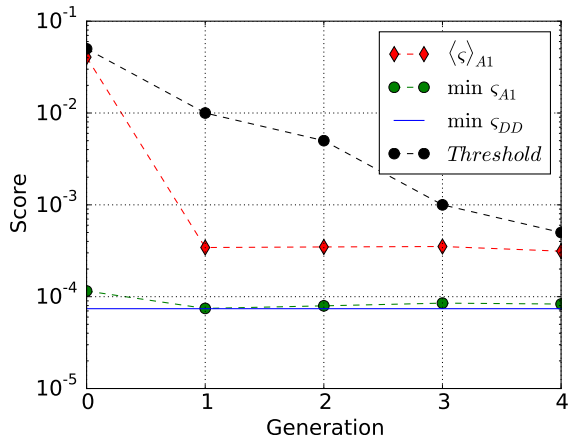
**CDD32** are length-32 concatenated sequences  $DD4[DD8]$  and  $DD8[DD4]$

**CDD64** are length-64 concatenated sequences  $DD4[CDD16]$  and  $DD8[DD8]$

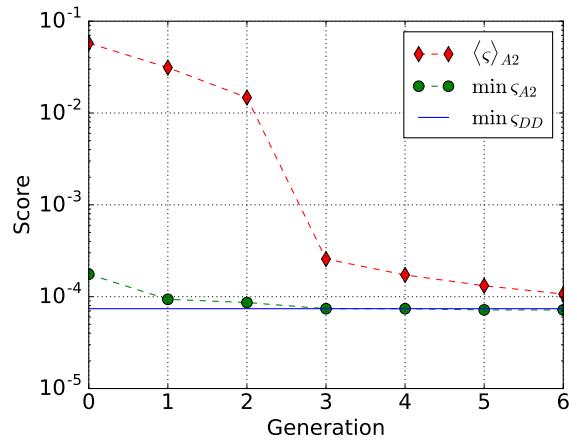
Longer DD-sequences can again be obtained by the concatenation of the ones listed above, and in the ideal situation they provide better and better protection against the noise. However, with realistic experimental capability, the performance usually saturates at a certain concatenation-level. Since at this moment we are only optimizing short DD-sequences, the listed ones are sufficient to provide a baseline for our purpose. One important family we did not include here is the “Knill DD” (KDD) [37], since it requires the use of non-Pauli gates. It is known that in some experiments, the KDD scheme helps to further increase the performance of CDD-sequences [44]. Thus, an interesting question is when given the freedom of applying non-Pauli gates and choosing variable lengths of the sequences, whether our algorithm could discover a similar strategy.

## B Additional Experiments

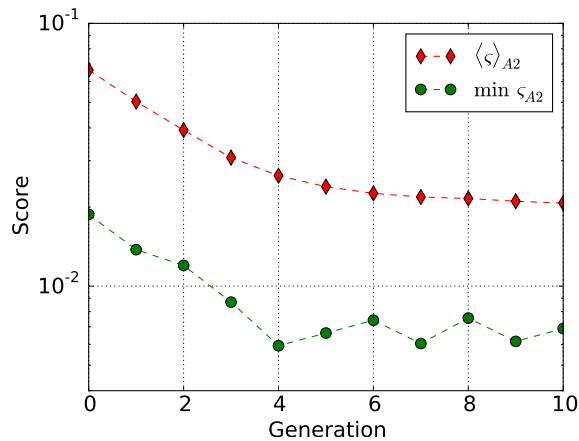
In this section we present the results of some additional experiments that have been done in the course of this work.



(a) Experiment B1



(b) Experiment B2



(c) Experiment B3

Figure 4: The three plots showing the convergence of the average and best scores of the data generated in Experiment B1-B3. The average score is computed on the training data set of each generation, which is the top 10% sequences generated by the selected models for B2 and B3 and the sequences with a score above the respective threshold for B1. (For generation 0, instead the training data is picked from randomly generated sequences). As a reference, also the best score obtained from DD is shown.

Sequences	$\langle \varsigma \rangle$	min $\varsigma$
CDD16	0.010699	<b>0.000074</b>
Last training set	<b>0.000313</b>	0.000083
Best model	0.004669	-
Random	0.125371	-

Table 5: A summary of the Experiment B1, with a comparison of the average score of the the best DD-family, the last training data, the best model of the last generation and random sequences. The sequences considered here consisted of 16 gates and  $\tau_d$  was set to 0.002. For the DD-scheme and the training data, also the best score is reported. The best results are printed bold.

**Exp. B1: Threshold** In this experiment, we considered sequences of 16 gates with  $\tau_d = 0.002$ . We employed Algorithm 1 and trained 300 models per generation for 50 epochs and chose the best 5 to generate the next training data. The number of generations was set to 4. Here we employed a marginally different version of Algorithm 1 in that we defined a threshold for the score of each generation’s training data and let the selected models generate 4000 sequences each with scores at least as good as the threshold. For the given number of gates and time step, we found the DD16-class contains the best sequences among the theoretical schemes explained in the Appendix A. The results are shown in Table 5, a plot of the average score of the generated data is shown in Figure 4a.

We can see both DD and our method produce good sequences for this scenario. However, similar to the experiments in the main text, the best model has a very remarkable average score and is able to generate sequences with large variety. What is also evident from the plot is that defining certain thresholds for the scores of each generation *a priori* is not a good strategy as it is very hard to infer how fast the average score will improve with the generations. In this case, the average score improved much faster as it was assumed and thus, the average score stagnated from generation one to four.

**Exp. B2: Percentage** We performed another experiment where we considered the same scenario as for the above experiment but used Algorithm 2 with an initial set of 30 networks from which we kept the best 5. From the data generated by the networks after each generation, we chose the best 10% as the new training data. The training data consisted of 10,000 sequences for each generation. Figure 4b and Table 6 show convergence and results.

As can be seen from the results, this experiment produced the best score we found for this scenario. Also the average score of the sequences of the last training data is about three times better than that of the previous experiment with thresholds. Note that these results were achieved by training a significantly lower number of networks.

**Exp. B3: Random Gates** In this experiment, we test the performance of Algorithm 2 when we replace the Pauli gates  $\{I, X, Y, Z\}$  with 10 randomly chosen gates, and each gate sequence has length-16. More precisely, each gate  $g_j$  is a randomly generated single qubit

Sequences	$\langle \varsigma \rangle$	min $\varsigma$
CDD16	0.010699	0.000074
Last training set	<b>0.000107</b>	<b>0.000072</b>
Best model	0.003046	-
Random	0.125371	-

Table 6: A summary of the Experiment B2, with a comparison of the average score of the best DD-family, the last training data, the best model of the last generation and random sequences. The sequences considered here consisted of 16 gates and  $\tau_d$  was set to 0.002. For the DD-scheme and the training data, also the best score is reported. The best results are printed bold.

unitary operator with eigenvalues 1 and  $-1$ , i.e.

$$g_j = U_j^\dagger X U_j, \quad \text{where } U_j \text{ is a random unitary.}$$

Other settings of the noise model and the control Hamiltonian remain unchanged, e.g. we use the same 4-qubit noise Hamiltonian, the control Hamiltonian is piecewise continuous and has the reversal symmetry. Also, the experiment is done with almost the same parameters as Experiment 3. The result is plotted in Figure 4c. We can see that the obtained DD-sequences with random gates have much worse performance compared to the ones with Pauli gates. Nevertheless, the use of neural networks allow us to sample better sequences over the generations. Thus, this experiment shows that the use of Pauli gates (combined with special length of sequences) is very useful prior knowledge. However, it also suggests that LSTM has the potential to handle a larger or even continuous set of gates for the dynamical decoupling problem, and therefore it is possible that our algorithm can be modified so that the LSTM could identify a good set of gates by itself.

## C Analysis

### C.1 Local correlations of DD sequences

As we suggested earlier, the reason we use RNNs as the probabilistic model is that the performance of dynamical decoupling sequences heavily depends on their local correlations. To illustrate this fact, we can count the frequency of length-2 (3) subsequences from the initial training set of the Experiment B1. More concretely, the training set is constructed by randomly generating sequences but only keeping ones with scores better than the threshold 0.05 (other parameters have been stated in the description of the experiment). We can then compare these statistics to the ones of the sequences generated by the LSTM, which is trained based on the training set. In table 7, we can see that the frequency of two



Next gate Previous	I	X	Y	Z
I	3.55% (3.39%)	6.04% (5.98%)	5.98% (5.69%)	5.97% (5.83%)
X	5.98% (5.93%)	6.45% (6.76%)	6.90% (7.11%)	6.86% (6.90%)
Y	5.99% (5.72%)	6.96% (7.21%)	6.34% (6.66%)	6.83% (6.80%)
Z	5.98% (5.48%)	6.74% (6.84%)	6.96% (7.24%)	6.44% (6.44%)

Table 7: The frequency of length-2 subsequences, from the initial training set and the set generated by the trained LSTM (given in parentheses). The total number of subsequences is 300,000.

Last gate Second	I	X	Y	Z
I	3.97% (3.75%)	6.19% (6.13%)	6.24% (5.73%)	6.34% (6.60%)
X	4.47% (4.49%)	5.37% (5.90%)	7.31% (7.25%)	7.26% (7.30%)
Y	6.67% (6.30%)	7.56% (7.75%)	7.07% (7.51%)	5.16% (5.22%)
Z	6.49% (6.12%)	7.25% (7.08%)	5.33% (5.61%)	7.30% (7.25%)

Table 8: The frequency of length-3 subsequences started with the gate  $X$ , from the initial training set and the set generated by the trained LSTM (given in parentheses). The total numbers of the subsequences started with  $X$  are 73,389 for the training set and 74,846 for the generated set.

consecutive  $I$  gates is significantly lower than other combination, which coincide with the fact that the “ $II$ ” combination appears very rarely in human constructed DD sequences.

To get more detail about local correlations, we could also count the frequency of length-3 subsequences (see table 8). For example, below the frequencies of subsequences starting with the  $X$ -gate are shown. It can be seen that the combination  $XII$  appears less often than others, which coincides with the 2-body statistics we listed above. Apart from that, we find that  $XIX$ ,  $XXX$ ,  $XYZ$ ,  $XZY$  occur less frequently than other combinations. This is probably due to the fact that these subsequences would only prove beneficial in specific situations. A full analysis however would require much more effort. We can find a similar level of disparity in the length-3 subsequences starting with  $I$ ,  $Y$  or  $Z$ . Based on the performance of RNNs when modelling English at the character-level [12], it is conceivable that this model can utilize these length-2(3) statistics for sampling good DD-sequences, thus improving the average performance.

Sequences	$\langle \varsigma \rangle$	$\min \varsigma$
EDD8	0.002781	0.002203
CDD32	0.053753	0.000432
Top 500 sequences	0.001081	0.000626

Table 9: A comparison between the scores of the top 500 DD sequences in the last generation of Experiment 2 and some DD families for the larger bath  $\dim(\mathcal{H}_{\mathcal{B}}) = 128$ . The best score of the 500 sequences is worse than best score of CDD32. However, it is clear that on average, the obtained sequences still work fairly well.

## C.2 Performance of the obtained sequences with a larger heat bath

In the main text, all the numerical simulations are done on a randomly generated noise Hamiltonian with the dimension of the bath being  $\dim(\mathcal{H}_{\mathcal{B}}) = 16$ . The small dimension of the bath is used in order to have a fast simulation. Here, we test the performance of some obtained sequences from the experiment 2, in the presence of a larger bath with  $\dim(\mathcal{H}_{\mathcal{B}}) = 128$ . Apart from the change of dimension, the Hamiltonian  $H_0$  is again randomly generated according to the description in 4.1, which has a 2-norm  $\|H_0\| = 24.0$ . We then computed the scores of the top 500 DD sequences in the last generation of Experiment 2. The results are shown in Table 9. While the best score of the obtained sequences is worse than best score of CDD32, it is clear that on average, the obtained sequences still work fairly well. This also suggests that our algorithm is potentially capable of adapting to the particular noise Hamiltonian, as the learned sequences outperform known DD-families in Experiment 2.

## D Best Sequences

We list here the best sequences we found in Experiment 1,2 and 3 from the numerical results section. We denote the identity by  $I$ ,  $X, Y, Z$  refer to the respective Pauli-matrices.

**Experiment 1**  $Z, Z, Y, X, Y, Z, Y, X, Y, Y, X, I, Z, X, Z, Z, Z, Z, X, X, Z, X, X, Y, X, Y, Y, X, I, Z, X, X$

**Experiment 2**  $Z, Y, Z, Y, Y, Z, Y, Z, Y, X, Z, X, Y, Y, X, Z, X, Y, Y, Z, Y, Y, Z, I, Y, Z, Y, I, Y, Z, Y, Y$

**Experiment 3**  $Y, Z, Z, X, X, Y, X, Y, Y, X, I, Z, Y, Y, X, Y, X, Z, X, X, X, Z, X, X, Z, Z, X, X, Y, X, Y, Y, X, I, I, Z, I, X, Y, X, I, Z, X, X, Z, X, Y, X, I, Y, Y, X, Y, X, X, Z, X, Z, X, Y, X, Z, X, Z$

## E Comparison of optimization algorithms

In this section, we will give a comparison between several optimization algorithms applied to black-box problems. In other words, the algorithm needs to optimize (minimize) the objective function  $f$  only by looking at the values of  $f(x)$  (without knowing the concrete formula of it). We are going to look at the following types of algorithms:

- Gradient-based algorithms, e.g. Newton’s method, variants of gradient descent.
- Metropolis-Hasting algorithms and its variants, e.g. simulated annealing
- Genetic algorithm and its variants, e.g. probabilistic model building genetic algorithm (PMBGA).

The performance of an optimization algorithm depends heavily on the class of the problems it is applied to. (This fact is known as the “no free lunch theorem for optimization”). Thus in the following, we will use different objective functions to illustrate the strong and weak points of those algorithms.

### E.1 Gradient based algorithms

To understand the idea of these algorithms, it is enough to consider  $f : \mathbb{R} \rightarrow \mathbb{R}$  defined on a single variable. The simplest gradient descent for finding the minimum of  $f$  is the following iterative algorithm: starting from a random number  $x_0$  and successively computing  $x_{n+1} = x_n - \alpha f'(x_n)$ . Gradient based algorithms perform well on functions with non-vanishing gradients almost everywhere and very few local minima, and likely have a poor performance otherwise. For example, the above algorithm would perform very well on a simple function  $f(x) = x^2$ , but much worse on the following fast oscillating function

$$f(x) = \sin(8x) + 0.5 \sin(4x) + 0.3 \sin(2x) + 0.1 \sin(x) \quad (2)$$

We plot the above function in Figure 5. It is easy to see we can construct  $f(x) = \sum_{i=1}^N a_i \sin(2^i x)$  such that the chance of finding the global minimum is arbitrarily small.

### E.2 Simulated annealing

Simulated annealing (SA) and its variants stem from the Metropolis-Hastings algorithm. The main idea is constructing a family of probability distribution  $p(x, T)$  based on the values of the objective function  $f(x)$ , with the requirement  $p(x, 0) > 0$  only when  $x$  is a global minimum of  $f$ . Then we repeatedly sample from  $p(x, T)$  while slowly decreasing  $T$ . In practice, simulated annealing is also an iterative algorithm, i.e. it chooses  $x_{n+1}$  based on  $x_n$ . Since SA uses the Metropolis-Hastings algorithm as a subroutine, there is a non-zero chance to choose  $x_{n+1}$  such that  $f(x_{n+1}) > f(x_n)$ . So in principle, SA could escape from local minima, which is an advantage compared to gradient descent. SA also works for functions with discrete variables. As a trade-off, it is likely to be slower compared to

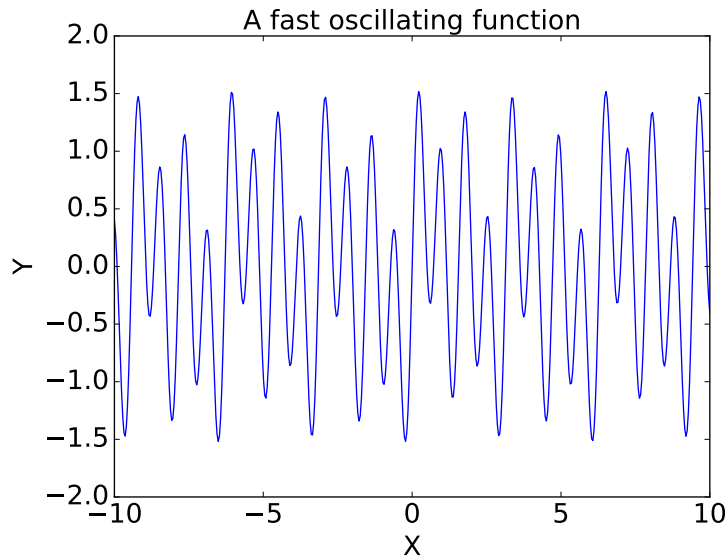


Figure 5: The plot of function (2).

gradient descent when  $f$  has very few local minima. Moreover, while SA has the mechanism to escape from local minima, in practice it could work poorly on functions with many local minima and high barriers between them, e.g. the Function (2).

### E.3 Genetic algorithms

In this subsection we will assume  $f$  has the form  $f : \mathbb{R}^N \rightarrow \mathbb{R}$ . A common feature in all versions of genetic algorithms (GA) is that they maintain a population of solutions  $\{\vec{x}_i, 1 \leq i \leq M\}$ , where  $\vec{x}_i = (x_{i1}, \dots, x_{iN})$ . For the first generation, a number of  $M' > M$  solutions is randomly generated, then we pick the  $M$  smallest  $f(\vec{x}_i)$  as the population. To generate new potential solutions for new generations, several different operations are introduced. In the original genetic algorithm, the two such operations are crossover and mutation. The effect of the mutation operation on a solution  $\vec{x}$  is

$$(x_1, \dots, x_j, \dots, x_N) \rightarrow (x_1, \dots, x'_j, \dots, x_N),$$

where  $x'_j$  is a random number. The crossover operation acts on two solutions  $\vec{x}$  and  $\vec{y}$

$$(\vec{x}, \vec{y}) \rightarrow (x_1, \dots, x_j, y_{j+1}, \dots, y_N),$$

where the position  $j$  is picked randomly. Then we can use these two operations to generate  $M''$  new test solutions from the first generation, combine them with the  $M$  old solutions and pick the top  $M$  solutions as the population of the second generation. Later generations can be obtained by repeating these steps.

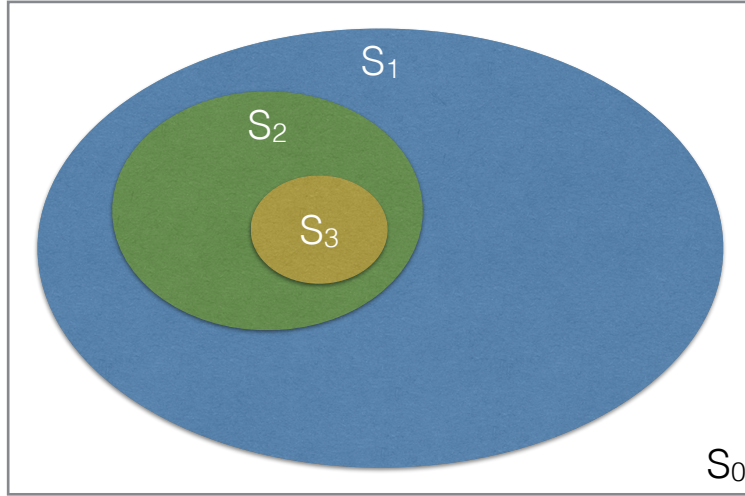


Figure 6: Sets  $S_i$  with better and better solutions.

To illustrate the advantage of the (original) genetic algorithm, we can consider the following objective function  $f$

$$f(\vec{x}) = \sum_j f_j(x_j) .$$

In this case, if  $f(\vec{x})$  is (relatively) small, then either  $\sum_{j=1}^k f_j(x_j)$  or  $\sum_{j=k+1}^N f_j(x_j)$  is (relatively) small. Thus the crossover operations serve as non-local jumps, while the mutation operations help to find local minimum. However, in general, it is not clear for what kind of function  $f$  the inclusion of the crossover operations could provide an advantage. It is easy to construct counter-examples such that the crossover operations deteriorate the performance, such as

$$f(\vec{x}) = f(\vec{x}_a, \vec{x}_b) = \|\vec{x}_a - \vec{x}_b\| ,$$

where  $\vec{x}_a, \vec{x}_b$  has equal dimension, and  $\|\cdot\|$  is the Euclidean norm. Clearly, in most cases, the crossover of two good solutions will only produce inferior new solutions.

It turns out that the most important feature of genetic algorithms is the use of a population. In comparison, other optimization methods we mentioned previously only keep track of the last test solution. If we are willing to believe that good solutions of the function  $f$  have a certain structure (thus partially dropping the black-box requirement of  $f$ ), it is possible that we can identify this structure from the solutions in the population, and then generate new test solutions. This idea has led to the so-called probabilistic model building genetic algorithm (PMBGA) and its variants [32, 31].

Instead of going through the details of these algorithms, we will explain the idea and the possible advantage via the following thought experiment. In Figure 6, let  $S_0$  be the set of all solutions, and  $\{S_i\}_{i \leq K}$  are the sets of solution with  $f(x) < \alpha_i$ , where  $\alpha_{i+1} < \alpha_i$ . Instead

of randomly searching for elements of  $S_K$ , we could first randomly search for elements of  $S_1$ . After having accumulated enough data of  $S_1$ , it is possible that we could build a probabilistic model of  $S_1$  that allows us to approximately sample from the set  $S_1$ . Applying this routine subsequently for each set  $S_i$ , we could obtain the model for  $S_K$  and sample from it. Assuming the order of these subsets satisfies  $|S_{i+1}| < \frac{1}{2}|S_i|$ , then in the ideal scenario the above iterative algorithm would provide an exponential speedup with respect to  $K$ . However, it is worth pointing out that automatically building a model from a data set is, in general, a difficult task (if possible at all).

As a concrete example, we can consider the objective function (2) and a routine  $A$  which looks for the periodicity of the data and then generates new test solutions accordingly. After we go through multiple generations, it is likely that the population would converge to the correct periodic subset that has the minimum  $f(x)$ .

## E.4 Summary

As seen in the discussion above, each of these optimization methods has its strong and weak points. Thus different methods are chosen depending on the prior knowledge we have on the concrete problems. It should be emphasized that we should not consider these methods as in a pure competition; instead, they can be used in complement with each other. For example, stochastic gradient Langevin dynamics (SGLD) [50] can be viewed as a combination of gradient descent and annealing, and in [33], it is mentioned that inclusion of the deterministic hill climber (discrete version of gradient descent) can lead to a substantial speedup in the PMBGA.

## F Machine Learning

This section will give a brief overview over the subfield of machine learning known as supervised learning and introduce a model for time-series data, known as Recurrent Neural Networks (RNN). Furthermore, some aspects of the optimization of this class of models will be elaborated on.

### F.1 Supervised Learning

The field of machine learning can be divided into three main subfields: supervised learning, unsupervised learning and reinforcement learning. These branches differ from each other by the way in which the respective models obtain information about the utility of their generated outputs.

In the case of supervised learning, it is assumed that for every input that a model shall be trained on, a "supervisor" provides a target, corresponding to the desired output of the model for the given input. These pairs of inputs and desired outputs are then used to make the model learn the general mapping between input and output.

More formally and from a Bayesian perspective, one assumes to have a dataset  $D$  of size  $N$ , consisting of several tuples of i.i.d. observations  $x \in \mathbb{C}^l$  and corresponding targets  $y \in \mathbb{C}^k$ , such that

$$D = \{(x_i, y_i) |_{i=1}^N\}$$

where  $x_i$  and  $y_i$  are instances of two random variables  $X$  and  $Y$  respectively. These random variables are assumed to be distributed according to some unknown probability distribution  $p_{Gen}$ , the so-called data-generating distribution,

$$X, Y \sim p_{Gen}(X, Y).$$

The goal of any supervised learning method now is to approximate the conditional distribution  $p_{Gen}(Y|X)$  in a way that allows for evaluation in some new observation  $x_* \notin \{x_i\}_{i=1}^N$ . Since  $p_{Gen}$  is not available, one resorts to fitting the empirical distribution  $p_{Emp}$  given by  $D$  as surrogate problem.

A typical way of deriving a concrete optimization-problem from this is to make an assumption regarding the form of  $p_{Gen}$  and treating the model at hand as a distribution  $p_M(Y|X, \Theta)$  of this kind, parametrized by the parameters of the model  $\Theta$  that are also often called the *weights* of the model. Now, the fitting of the model can be perceived as a maximum-likelihood problem and hence the supervised learning problem can be formulated as

$$\max_{\Theta} \mathcal{L}(\Theta|D) = \max_{\Theta} \prod_i p_M(y_i|x_i, \Theta),$$

making use of the i.i.d.-assumption. A commonly employed trick to obtain a more benign optimization problem is to instead optimize the *negative log-likelihood*. As the logarithm is a monotonic function, this transformation does not change the location of the optimum in the error landscape, but turns the product of probabilities into a sum over the tuples in  $D$ . This step then yields a minimization problem, given by

$$\min_{\Theta} - \sum_i \log p_M(y_i|x_i, \Theta).$$

Alternatively, one may also minimize

$$\min_{\Theta} - \frac{1}{N} \sum_i \log p_M(y_i|x_i, \Theta)$$

which is called *empirical risk minimization* (ERM). These statements of the problem can now be tackled with the optimization methods appropriate for the given model. In the case of the RNN, gradient-based optimization is the state-of-the-art approach and will be explained in Section F.3.

While it is obvious that fitting a model with respect to  $p_{Emp}$  is identical to fitting it to  $p_{Gen}$  as long as every tuple in  $D$  is only considered once, this is not necessarily true anymore when considering each tuple multiple times. This however is needed by many models in order to fit their parameters to a satisfying degree. In order to prevent the model

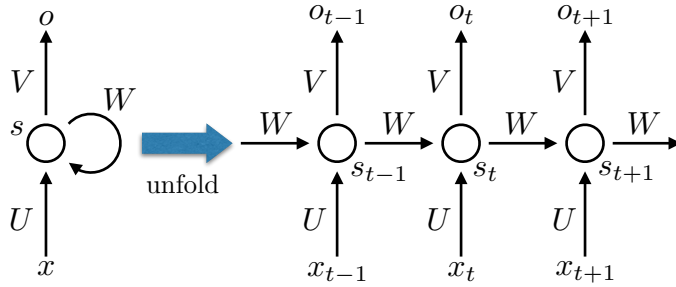


Figure 7: The standard model of a Recurrent Neural Network shown for three time-steps.

from learning characteristics of the empirical distribution that are not present in the data-generating distribution, a phenomenon commonly known as *over-fitting*, often some form of regularization is applied. This may be done by punishing too large parameter values, stopping the training after performance starts to decrease on some hold-out data set or by averaging over multiple models. Note that in the Bayesian picture some penalty-terms can be perceived as the logarithm of a prior distribution over  $\Theta$ , hence turning the optimization problem into finding the *maximum a-posteriori* parameters.

## F.2 Recurrent Neural Networks

In this section, the Recurrent Neural Network model will be introduced. We will start with an introduction of the standard version of the model and based upon this, explain the advanced version of the model employed in this work in a second step.

### F.2.1 The Standard RNN Model

In many areas of application, the data can be perceived as, often non-Markovian, discrete time-series data, such that an observation  $x_t \in \mathbb{R}^l$  at some time  $t$  depends on the previous observations  $x_{t-1}, \dots, x_1$  or with respect to the framework introduced above,

$$X_t \sim p(X_t | X_{t-1}, \dots, X_1).$$

While Markov Chains have been the state-of-the-art approach for this kind of data during the last decades, with the recent rise of artificial neural networks, RNNs [53, 51] have also gained momentum and are now generally considered to be the most potent method.

A RNN is defined by the two non-linear maps  $s_t : \mathbb{R}^l \rightarrow \mathbb{R}^h$  and  $o_t : \mathbb{R}^h \rightarrow \mathbb{R}^o$  given by

$$\begin{aligned} s_t &= f_s(Ux_t + Ws_{t-1} + b_s) \\ o_t &= f_o(Vs_t + b_o), \end{aligned}$$

where  $U \in \mathbb{R}^{h \times l}$ ,  $W \in \mathbb{R}^{h \times h}$ ,  $V \in \mathbb{R}^{o \times h}$ ,  $b_s \in \mathbb{R}^{1 \times h}$ ,  $b_o \in \mathbb{R}^{1 \times o}$  and the trainable parameters of the models are constituted by  $\Theta = \{U, V, W, b_s, b_o\}$ . The non-linear function  $f_s$  is often



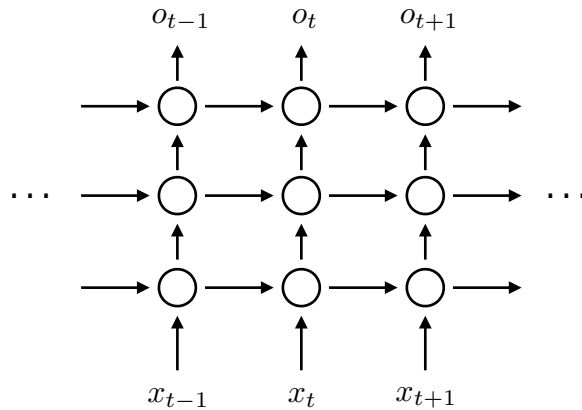


Figure 8: An illustration of an RNN with 3 hidden layers.

chosen to be  $\tanh$ , the rectifier-function given by

$$\text{rect}(x) = \max(0, x)$$

or the sigmoid-function given by

$$\text{sigm}(x) = \frac{1}{1 + e^{-x}}.$$

The function  $f_o$  must be chosen according to the distribution that is to be approximated by the model. For the case of a multinoulli-distribution as assumed in this work, the corresponding function would be the *softmax*, defined as

$$\text{softmax}(x)_j = \frac{e^{x_j}}{\sum_k e^{x_k}},$$

the superscripts in this case denoting the single elements of the vector  $x$ .

The intuition behind this simple model is that it combines its information about the input at a given time step with a memory of the previous inputs, referred to as *state* of the network. The precise nature of this combination and the state depends on the weight matrices  $U$  and  $V$  and the bias-vector  $b_s$ . The combined information is then used as input of the chosen non-linear function  $f_h$  to generate the next state. From this state, the output  $o_t$  is then computed as defined by  $W$ ,  $b_o$  and  $f_o$ . The effect of an RNN acting on the sequence  $\{x_t\}$  is illustrated in Figure 7.

From the above explanation, it is clear that the power of the model depends strongly on the size of the hidden state  $h$ . It should however also be noted that another effective way of increasing the expressive power of an RNN is to construct a composition of multiple functions of the form of  $s_t$ , see Figure 8. In the machine learning terminology, the respective functions are called the *layers* of an artificial neural network and the number of composed functions is referred to as the depth of a network. The layers between the input and the output are referred to as *hidden layers*. The common intuitive reasoning behind stacking

multiple layers is that it will allow the network to learn a hierarchy of concepts, called *features*, from the initial input data. Thereby, the features are assumed to be of increasing complexity with every layer, as they are based on a linear combination of the features learned by the layer below. Apart from this intuitive reasoning, also more rigorous work on the benefits of using at least one hidden layer between input and output can be found in the literature [3, 17, 16]. This ansatz of increasing the power of neural network models via deepening their architecture is publicly known as *Deep Learning* and has led to a drastic increase in success of machine learning methods during the last decade. However, having a composition of many state-computing functions of similar size can slow down the optimization process. This is why, when forming such a composition, each pair of functions is often connected via a simple linear projection from the space of the state of the earlier function onto some lower-dimensional space that is then used by the following function. Note that while all the above claims seem natural and lead to a good enough performance for our paper, more benchmarking is needed to really confirm them.

Now, in the case of supervised learning, one assumes to be in possession of a set of time-series  $x_1, \dots, x_n$  that shall be used to let the RNN learn to predict series of this kind. The natural way of doing this is to define the pairs  $(x_i, y_i) := (x_t, x_{t+1})$ . While in principle the model is capable of taking into account all previous time steps, in practice it shows that optimization is only feasible for a relatively short number of steps. This is mainly due to the fact that the gradients that are needed to optimize the parameters of an RNN tend to grow to infinity or zero for higher numbers of steps. This will be discussed more in-depth below.

### F.2.2 Long Short-Term Memory Networks

In order to improve upon the standard RNN, Hochreiter et. al. introduced the Long Short-Term Memory network (LSTM) [15], which provides a different way of computing the state of an RNN. Hence the following set of equations can be perceived as a replacement for  $s_t$  from the previous section. The main advantage of the approach is that it drastically mitigates the problem of unstable gradients by construction. It is defined by the following set of equations,

$$\begin{aligned}
 i_t &= \text{sigm}(U^i x_t + W^i s_{t-1} + b^i) \\
 f_t &= \text{sigm}(U^f x_t + W^f s_{t-1} + b^f) \\
 o_t &= \text{sigm}(U^o x_t + W^o s_{t-1} + b^o) \\
 \tilde{c}_t &= \text{tanh}(U^{\tilde{c}} x_t + W^{\tilde{c}} s_{t-1} + b^{\tilde{c}}) \\
 c_t &= c_{t-1} * f_t + \tilde{c}_t * i_t \\
 s_t &= \text{tanh}(c_t) * o_t
 \end{aligned} \tag{3}$$

where again  $x_t$  is the input at time step  $t$ ,  $s_{t-1}$  is the previous state of the network and  $c_t$  is the state of the cell.  $U^i, U^f, U^o, U^{\tilde{c}} \in \mathbb{R}^{h \times l}$ , while  $W^i, W^f, W^o, W^{\tilde{c}} \in \mathbb{R}^{h \times h}$ ,  $b^i, b^f, b^o, b^{\tilde{c}} \in \mathbb{R}^{1 \times h}$  and  $*$  denotes the element-wise multiplication.

As it can be seen from the equations, the way in which an LSTM computes the state is a bit more involved. If needed, it may however just be treated as a black box and can be

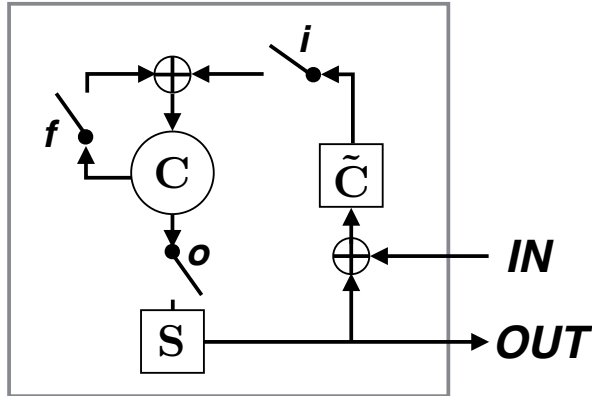


Figure 9: The Long Short-Term Memory model illustrated in a schematic way. In addition to the diagram above, the input gate  $\mathbf{i}$ , the forget gate  $\mathbf{f}$  and the output gate  $\mathbf{o}$  all depend on the current input  $x_t$  and previous state of the network  $s_{t-1}$ , as described in (3).

stacked just in the same manner as it was described for the plain RNN model. The general idea of an LSTM is to give the model a higher degree of control over the information that is propagated from one time step to the next. This is achieved by making use of so-called *gates* that control the information flow to and from the network and cell state. These gates, by taking into account the previous state and the new input, output vectors of values in  $[0, 1]$  that determine how much information they let through. In the equations given above,  $i_t$  is called the *input gate*,  $f_t$  is referred to as the *forget gate* and  $o_t$  denotes the *output gate*. Now, the mechanism works as follows:

- For a given time step  $t$ , the new input and previous network state are processed by  $\tilde{c}_t$  like for the standard RNN and the output values are squashed to the interval  $[-1, 1]$  to yield candidate values for the next cell state.
- The input gate  $i_t$  determines how to manipulate the information flow from the candidate cell state. Likewise, the forget gate  $f_t$  determines how to affect the information flow from the old cell state. The gated previous cell state and the gated input are then added to form the new cell state  $c_t$ .
- Finally, the output gate  $o_t$  determines what to output from the new cell state. The new cell state is then also projected onto the interval  $[-1, 1]$  and put through the output gate to become the network state.

The whole process is shown in Figure 9.

Naturally, there exists a plethora of possibilities to adapt the normal LSTM as explained above. One important enhancement is commonly referred to as *peepholes*, which allows the gates to incorporate the cell state via an extra term in the sum, in addition to the input and the network state. One other popular possibility introduced in [39] is the use

of projection layers between different time steps of LSTM. In this case, we replace  $s_{t-1}$  by  $r_{t-1}$  in the equations for  $i_t, f_t, o_t$  and  $\tilde{c}_t$  and add the simple equation

$$r_t = W^p s_t$$

where  $W^p \in \mathcal{R}^{k \times h}$  is the projection matrix. In this work, we have made use of both of these extensions of the normal LSTM. For an exhaustive overview over the known variants of the LSTM, we refer the interested reader to [13].

### F.3 Optimization of RNNs

As the optimization problem described in the beginning of this section can not be solved analytically for the models considered in this work, gradient-based approaches have established themselves as the state of the art. However, in the case of fitting the parameters of neural network models, three main restrictions need to be accounted for:

1. The number of parameters for neural network models easily exceeds 100,000 and can for larger architectures go up to several tens or even hundreds of millions. Hence, computing the Hessian (or its inverse) explicitly is not tractable and so, one is limited to first-order or approximative second-order methods.
2. As the error function that is minimized is only a surrogate error function, its global optimum is not necessarily the optimum of the error function one actually wants to minimize.
3. For many real-world data sets, computing the gradient of the complete sum of the error function over all samples is not feasible. Hence, the sum is normally split up into smaller parts called *mini batches* and these batches are looped over. A complete loop over  $D$  is then called an *epoch*.

These restrictions have led to the rise of an own subfield of machine learning that is concerned with the parallelization of gradient computations in the mini batch case, the approximation of second-order information and the formal justification for the splitting up of the error function. All of the currently available methods are nevertheless extensions of the simplest method for gradient-based optimization known as *steepest gradient descent*: At iteration  $i$  in the loop over the batches, the parameters  $\Theta$  are updated according to

$$\Theta_{i+1} = \Theta_i - \gamma \frac{\partial \mathcal{E}}{\partial \Theta_i}$$

where  $\mathcal{E}(D, \Theta)$  is the respective error function and  $\gamma$  is called the *step rate*. The most straight forward natural adaption is to make  $\gamma$  depend on the iteration and slowly decrease it over time, following the intuition that smaller steps are beneficial the closer one gets to the respective optimum. In addition to that, many methods employ some kind of momentum term [45] or try to approximate second order information and scale the gradient accordingly [46, 22].

Besides this, the size of the batches also has an influence on the performance of the respective optimization method. In the extreme case where each batch only consists of one sample, the gradient descent method is known to converge almost surely to an optimum under certain constraints [38]. As picking individual samples for optimization can be perceived as sampling from the empirical distribution to approximate the overall gradient, this method is called *stochastic gradient descent* (SGD). Using single data points however is computationally inefficient and by definition leads to heavily oscillating optimization, so it is common practice to resort to larger batches. Following the ERM-interpretation, batches  $B$  consisting of  $S_B$  samples are often used to compute an approximation of the mean gradient over  $D$  given by

$$\left\langle \frac{\partial \mathcal{E}}{\partial \Theta_i} \right\rangle_D \approx \left\langle \frac{\partial \mathcal{E}}{\partial \Theta_i} \right\rangle_B = \frac{1}{S_B} \sum_{(x,y) \in B} \frac{\partial \mathcal{E}_{(x,y)}}{\partial \Theta_i}$$

where obviously

$$\lim_{|B| \rightarrow |D|} \left\langle \frac{\partial \mathcal{E}}{\partial \Theta_i} \right\rangle_B = \left\langle \frac{\partial \mathcal{E}}{\partial \Theta_i} \right\rangle_D.$$

This interpretation is used, e. g. by the recently proposed algorithm *Adam* which has been shown to yield very good local optima while being very robust with respect to noisy gradients and needing comparatively little adjustment of its parameters. We have employed Adam for fitting the models used in this work.

While the approach to optimizing artificial neural networks is well established, this does not change the fact that the optimization problems posed by them are inherently difficult. It is well known that the error landscape becomes less smooth the more layers one adds to a network. This results in error surfaces with large planes where  $\frac{\partial \mathcal{E}}{\partial \Theta} \approx 0$  that are followed by short but very steep cliffs. If the step rate is not adapted correctly, the optimization procedure is very likely to get stuck in one these planes or saddle points and to jump away from an optimum in the vicinity of  $\Theta$  if evaluated on one of the cliffs. The phenomena of the frequent occurrence of very large or very small gradients are referred to in the literature as the *exploding gradient* or *vanishing gradient* problem respectively. To get a better understanding of why these problems exist, it is instructive to examine how the gradients for a given model are obtained.

As has been explained above, multi-layer neural network models are a composition of non-linear functions  $\mathbb{R}^{i_k} \rightarrow \mathbb{R}^{o_k} : x_{k+1} = f_k(W_k x_k + b_k)$ , where  $W_k$  is the weight-matrix,  $b_k$  the bias-vector,  $x_0$  the input data and  $x_K$  the final output of the network. From this definition it is clear that  $o_k = i_{k+1}$ . For convenience, we define  $y_k \equiv W_k x_k + b_k$ . In order to obtain the gradient for a specific  $W_k$  or  $b_k$  one must obviously make use of the chain rule, such that

$$\frac{\partial \mathcal{E}}{\partial W_k} = \frac{\partial \mathcal{E}}{\partial x_{k+1}} \frac{\partial x_{k+1}}{\partial y_k} \frac{\partial y_k}{\partial W_k} = \frac{\partial \mathcal{E}}{\partial x_K} \left( \prod_{j=k+1}^{K-1} \frac{\partial x_{j+1}}{\partial x_j} \right) \frac{\partial x_{k+1}}{\partial y_k} \frac{\partial y_k}{\partial W_k}$$

and

$$\frac{\partial \mathcal{E}}{\partial b_k} = \frac{\partial \mathcal{E}}{\partial x_{k+1}} \frac{\partial x_{k+1}}{\partial y_k} \frac{\partial y_k}{\partial b_k} = \frac{\partial \mathcal{E}}{\partial x_K} \left( \prod_{j=k+1}^{K-1} \frac{\partial x_{j+1}}{\partial x_j} \right) \frac{\partial x_{k+1}}{\partial y_k} \frac{\partial y_k}{\partial b_k}$$

where  $\frac{\partial}{\partial W_k}$  is the shortcut of doing the derivative element-wise:

$$\left[ \frac{\partial}{\partial W_k} \right]_{ab} = \frac{\partial}{\partial [W_k]_{ab}}$$

The same convention applies to  $\frac{\partial}{\partial b_k}$ . As  $\frac{\partial}{\partial W_k}$  and  $\frac{\partial}{\partial b_k}$  depend on all the gradients of the later layers, this formulation yields an efficient method of computing the gradients for all layers by starting with the uppermost layer and then descending in the network, always reusing the gradients already computed. Together with the fact that many of the commonly used non-linearities have an easy closed-form expression of the first derivative, this allows for fully automatic computation of the gradients as it is done in every major deep learning framework. This dynamic programming method of computing the gradients is known in the literature as *Back-Propagation*. The vanishing (exploding) gradient problem arises because of the product  $\prod_{j=k+1}^{K-1} \frac{\partial x_{j+1}}{\partial x_j}$  in the above equations. For example, if one of the  $\frac{\partial x_{j+1}}{\partial x_j} \approx 0$  in the product, then likely we have  $\frac{\partial \mathcal{E}}{\partial W_k} \approx 0$ , which leads to an ineffective gradient descent. Similarly, if many of the terms  $\frac{\partial x_{j+1}}{\partial x_j}$  have large norms, then there is a possibility that  $\frac{\partial \mathcal{E}}{\partial W_k}$  becomes too large, which often causes the optimization method to jump out of a local optimum.

In the case of an RNN as defined in Section F.2, the above generic equations for the derivative become a little more involved, as in addition to the term for possibly multiple stacked layers, a term accounting for states of previous times has to be added. Nevertheless, at the heart of the problem, it is still about computing derivatives of composite functions. This slightly more involved back-propagation method is known as *Back-Propagation through Time* and can also be fully automatized. Similar to the multi-layer neural network models mentioned above, the gradient computation of RNNs also has these instability issues. As can be seen from Figure 7, the same matrix  $W$  is used in all time step of an RNN. Thus, a tiny change of  $W$  could affect the output  $o_t$  drastically when the time step  $t$  gets big. In other words, the derivative of the error function  $\mathcal{E}$  with respect to  $W$  could again become very large or very small in certain situations. To deal with this issue, we could truncate the number of time steps during the computation, as described in Figure 10. More discussion on this topic can be found in Section 3.2 of [12].

## G Technical Aspects

For the implementation of this work, we have made use of Python with the numerical libraries NumPy, SciPy and TensorFlow [48, 18, 1]. All experiments were run on single workstations with up to 8 threads. The runtime of the experiments varied, depending on the optimization parameters, from a few hours to several days.

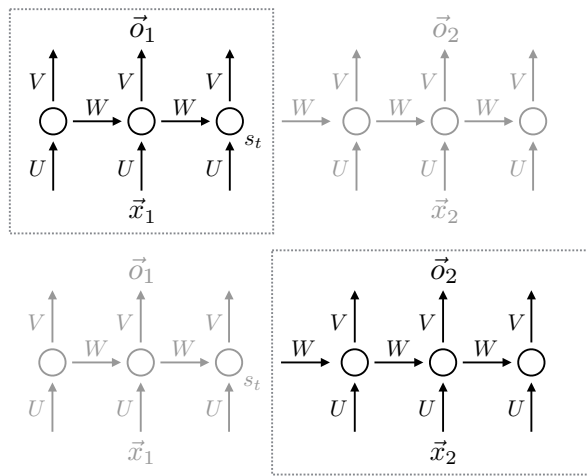


Figure 10: An illustration of how we truncate the gradient computation for long sequences. Here we divide the sequences into two halves. As the first step, we compute the gradient of the error function  $\mathcal{E}(\vec{x}_1, \vec{o}_1)$  with respect to the parameters  $U, V, W$ , while ignoring the other half of the network. In the second step, we compute the gradient of  $\mathcal{E}(\vec{x}_2, \vec{o}_2)$ , while treating the final state of the network  $s_t$  of the first half as a constant. The final gradients are approximated by the sums of these two constituents. Thus, we are able to avoid the instability of computing gradients, but still capture the correlation between two halves, since we feed the final network state  $s_t$  into the second half.